Cerebral Hemodynamics and Cerebral Blood Volume: MR Assessment Using Gadolinium Contrast Agents and T1-Weighted Turbo-FLASH Imaging

Bruce L. Dean,[1] Charles Lee,[2] John E. Kirsch,[2] Val M. Runge,[2] Robert M. Dempsey,[3] and Luther C. Pettigrew[4]

Purpose: To assess the degree and regional pattern of first-pass brain enhancement using dynamic MR imaging. **Materials and Methods:** Ultrafast MR imaging (1.06-second acquisition time per image) was performed in 19 healthy subjects following a bolus IV injection of a gadolinium contrast agent; 36 patients with suspected pathology were studied using the same protocol. **Results:** Calculated percent blood volumes were 4.9% for right cortical gray matter, 4.8% for left cortical gray matter, and 2.6% for white matter. Subtraction images were obtained that depicted the first pass "blood pool" pattern of enhancement (gray and white matter) which was significant. **Conclusion:** Preliminary evidence suggests utility for cerebral "blood pool" imaging, especially if reduced image acquisition times can be achieved.

Index terms: Magnetic resonance, flow studies; Magnetic resonance, technique; Blood, magnetic resonance; Cerebral blood, flow; Cerebral blood, volume

AJNR 13:39–48, January/February 1992

Imaging of brain hemodynamics and calculations of cerebral blood flow (CBF) and cerebral blood volume (CBV) have been assessed by many methods, such as, contrast computed tomography (CT) with dynamic bolus techniques (1–7), stable (8–10) and radioactive (11) xenon methods, rapid sequence digital subtraction angiography (12–15), positron emission tomography (PET) (16, 17), and single photon emission computed tomography (SPECT) (18, 19). There is high anatomic resolution with CT, but limited immediate cortical enhancement following a contrast bolus that lessens its clinical utility. Xenon CT and PET are not routinely available in most institutions, and SPECT does not have the resolution associated with CT or magnetic resonance imaging (MR).

With the advent of "ultra-fast" MR imaging techniques, a dynamic assessment of intracranial hemodynamics is possible following an intravenous injection of a gadolinium agent. MR, similar to dynamic contrast-enhanced CT, allows high anatomic resolution but, additionally, a greater magnitude of first-pass enhancement. The first-pass enhancement reflects the initial transit of "contrast" through the vascular system, as opposed to conventional enhancement which suggests an incomplete blood-brain barrier.

The purpose of this study is primarily to characterize normal patterns and degree of immediate, first-pass brain enhancement with the T1-weighted method following a bolus of intravenous gadolinium agent and to calculate percent blood volumes of cortical gray matter and white matter. Secondarily, 36 patients with suspected pathology were reviewed and anecdotal examples from this group are presented. Subtraction techniques (postcontrast minus precontrast images) may be utilized to depict the regional cerebral "blood pool"

Received January 14, 1991; revision requested April 10; revision received June 17; final acceptance June 27.

Presented at the 28th Annual Meeting of the ASNR, Los Angeles, CA, March 19–23, 1990.

This work was supported in part by a Clinical Investigator Development Award, NINDS/NIH 1 K08 NS1505-01, to L.C.P.

[1] Barrow Neurological Institute, St. Joseph Hospital and Medical Center, 350 West Thomas Rd., Phoenix, AZ 85013. Address reprint requests to B. L. Dean.

[2] Department of Diagnostic Radiology, Magnetic Resonance Imaging and Spectroscopy Center, University of Kentucky Medical Center, Lexington, KY 40536-0084.

[3] Department of Neurosurgery, Magnetic Resonance Imaging and Spectroscopy Center, University of Kentucky Medical Center, Lexington, KY 40536-0084.

[4] Department of Neurology, Magnetic Resonance Imaging and Spectroscopy Center, University of Kentucky Medical Center, Lexington, KY 40536-0084.

AJNR 13:39–48, Jan/Feb 1992 0195-6108/92/1301-0039

pattern approximating the volume of vascular distribution in a region of brain.

Subjects and Methods

Subjects

Nineteen subjects ranging in age from 28 to 68 years (mean age 55 years) were enrolled in the study. There were 11 men and 8 women. All patients were presumed to have normal CBF. Patients, in general, were scanned for noncirculatory related diagnoses (ie, rule-out acoustic neuroma, headaches, etc). All patients had been scheduled for contrast scans by their referring physicians. The Turbo-FLASH sequence was added as a modification to the usual protocols. Additionally, 36 patients with a suspicion of altered brain hemodynamics or mass lesions were studied by the same protocol to initially assess the clinical relevance of the study method.

Contrast Injection

Eight mL of gadopentetate dimeglumine (Magnevist, Berlex, Wayne, NJ) were injected in 18 patients in approximately 5–10 seconds, followed by saline to clear the line of contrast material. One patient was administered an equivalent dose of gadoteridol (ProHance, Squibb, Princeton, NJ). Intravenous lines were placed, when possible, in the antecubital fossa. The contrast was injected at the port closest to the intravenous site. The contrast injection was initiated concurrently with the first scan (snap-shot image). The intravenous injection was accomplished by a 20-mL syringe "by-hand."

Scanning Procedure

Scans were initiated at preselected levels of the basal ganglia or lateral ventricles. Each "snap-shot" image had an acquisition time of 1.06 seconds. There was an interimage delay time of 1.5 seconds. Total acquisition time for the sequence of 20 images was 49.7 seconds. Additional parameters include: 8/4/1 (TR/TE/excitations), $\Theta = 10°$, field of view = 250 mm, matrix = 128 × 128, 1-cm thickness. A heavily T1-weighted scan was acquired with a preparatory 180° inversion pulse (Fig. 1). An effective inversion time (TI) of 529 msec was achieved for the scanning sequence. Scans were obtained by a Siemens 1.5 T system. Baseline and postcontrast images are presented in Figure 2.

Measurement of Enhancement

Regions of interest (ROIs, Fig. 2) were obtained of cortical gray matter in each hemisphere, deep white matter, superior sagittal sinus (SSS), and background signal. Reliable ROIs of arterial structures could not be obtained due to their relatively small size. Large ROIs were obtained to mitigate the high pixel statistical fluctuation. The mean

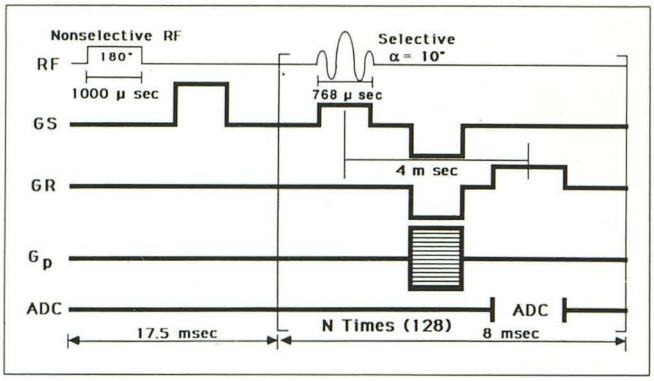

Fig. 1. Nonselective 180° inversion pulse is applied for a heavily T1-weighted image 8/4/1.

number of pixels per ROI was 100 (4.0 cm^2) for right cortical gray matter, 110 (4.4 cm^2) for left cortical gray matter, 43 (1.7 cm^2) for white matter, and 245 (9.8 cm^2) for background signal. ROIs were placed to lessen partial-volume effects with adjacent regions. The sagittal sinus enhancement was measured by four pixels to lessen partial-volume effects (0.16 cm^2). The background signal was obtained at each signal intensity baseline measurement. There were small variations in the background signal intensities during the scan sequence. Square, rectangle, or circular ROIs were used, as needed. Asymmetrical shaped or sized ROIs were used in opposite hemispheres, at times, to lessen partial-volume effects. ROIs for cortical gray matter were placed over the posterior frontal or anterior parietal areas. White matter was evaluated in the region of the major and minor forceps areas. Mean signal intensities were obtained for all twenty images. Graphs of signal intensities were obtained by a point-to-point method (Fig. 3). Percent enhancement was calculated by:

$$\%\text{Enhancement (peak)} = \frac{\text{SI (peak of curve)} - \text{SI (baseline)}}{\text{SI (baseline)} - \text{Background}} \times 100 \quad \text{(A)}$$

where SI = signal intensity.

First-order slopes were calculated from the points of peak enhancement and baseline points for gray and white matter. Blood volumes were calculated for gray and white matter by the following equation:

$$\%\text{rCBV} = \frac{\int_{\text{baseline SI}}^{\text{peak SI}} \text{SI(t)}_{\text{brain}}\,dt \times 0.85 \times 100}{\int_{\text{baseline SI}}^{\text{peak SI}} \text{SI(t)}_{\text{blood}}\,dt \times \text{DF} \times 0.7} \quad \text{(B)}$$

where 0.85 = cerebral to large vessel hematocrit correction factor; DF = dilution factor of blood by contrast; 0.7 = SSS flow-related enhancement correction; SI blood = measured over the sagittal sinus; rCBV = regional cerebral blood volume.

Calculations of %CBV were performed by measuring the areas under the generated curves from baseline to peak

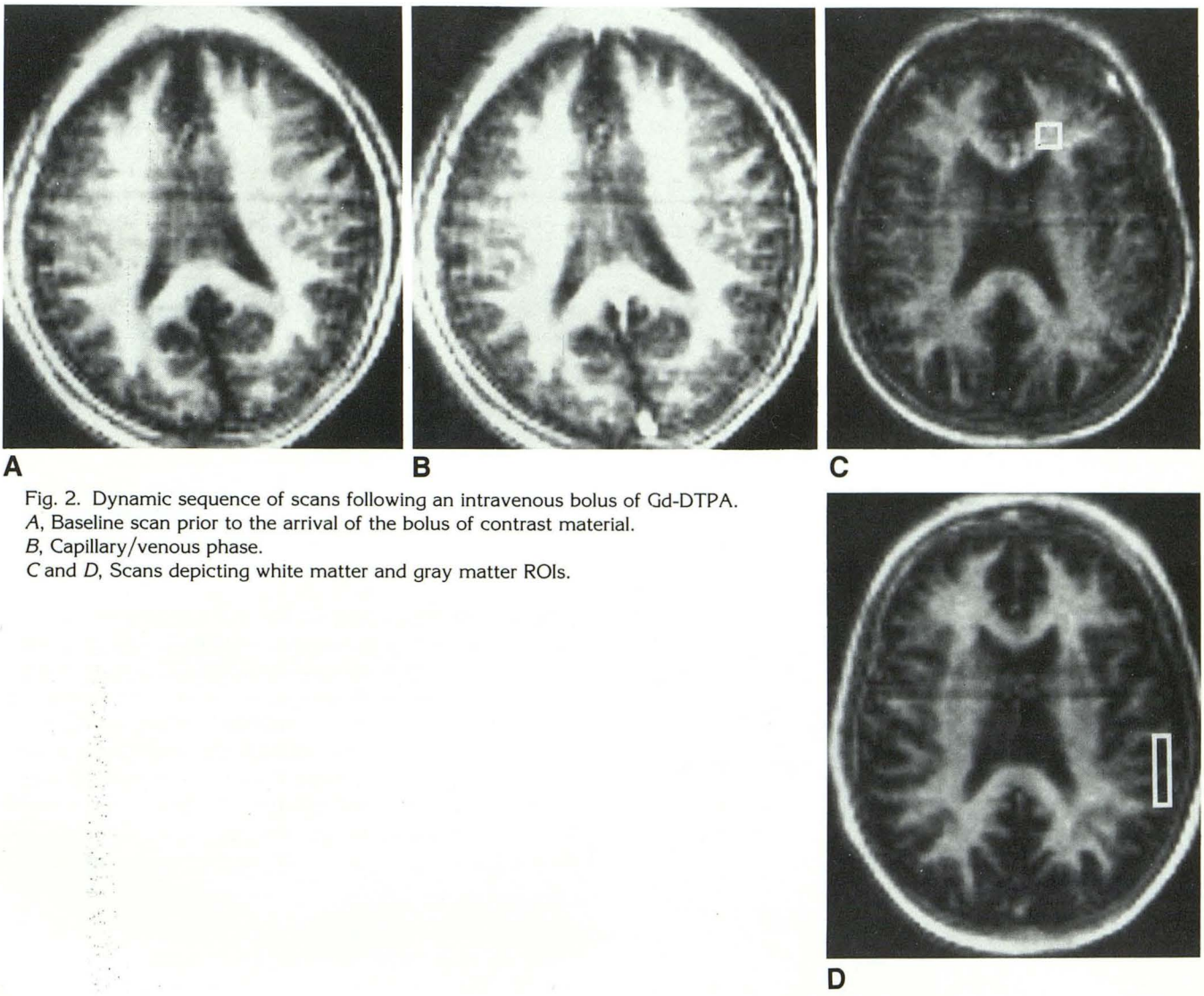

Fig. 2. Dynamic sequence of scans following an intravenous bolus of Gd-DTPA.
A, Baseline scan prior to the arrival of the bolus of contrast material.
B, Capillary/venous phase.
C and *D*, Scans depicting white matter and gray matter ROIs.

enhancement. The curves do not return to baseline after passage of the bolus due to recirculation and a noncompact bolus, as opposed to a compact arterial bolus or central venous bolus. This necessitates measuring from baseline to peak enhancement rather than the complete curve.

Calibration of SSS Flow-Related Enhancement

Calculation of SSS flow-related enhancement was derived from a signal intensity versus velocity plot. SSS flow was simulated by placing a 9-mm (inner diameter) tubing longitudinally through the scanner. Outdated blood (2.5 L) with 1 mmol/L concentration of Gd-DTPA was pumped over a range of velocities by a Sarns cardiovascular pump (Ann Arbor, MI). There was a mild pulsatile component to the flow that was dampened by the 20 meters of tubing. Five data points were obtained for each velocity. Our standard T1-weighted Turbo-FLASH sequence was used to evaluate the signal intensity for each velocity. The central four pixels were measured to simulate the central flow in the SSS. The central pixels were chosen to lessen laminar flow effects near the walls. The SSS flow-related enhancement factor was calculated by dividing the signal intensity (SI) of stationary blood by the SI of flowing blood at the physiologic velocities of the SSS (Fig. 4).

Correction Factor SSS Flow-Related Enhancement

$$= \frac{SI_{\text{stationary blood}}}{SI_{\text{blood at 20–40 cm/sec}}} \quad \text{(C)}$$

These calculations are valid only for this sequence and its corresponding parameters (ie, TR and slice thickness).

Results

First-pass enhancement of cortical gray matter, white matter, and sagittal sinus are tabulated in Table 1. Average enhancements were: 1) right

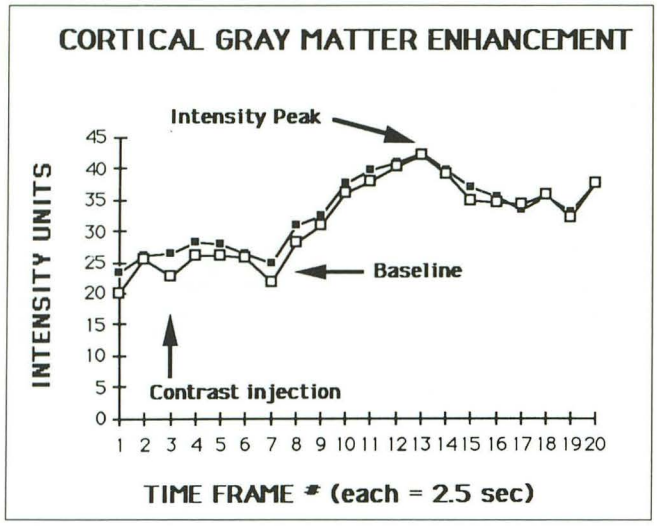

Fig. 3. Point-to-point graph of right and left cortical gray matter enhancement for patient 5.

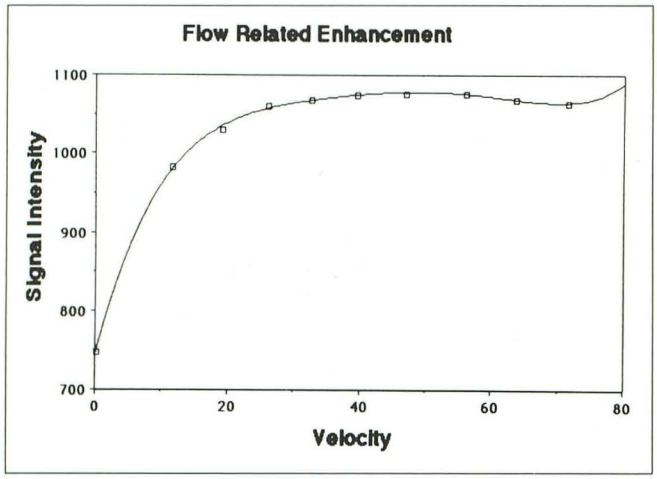

Fig. 4. Plot of the flow-related enhancement of the SSS. The response of signal intensity to velocity is depicted from 0 to 70 cm/sec for whole blood with 1 mmol/L of Gd-DTPA.

gray matter: 12.4 SI units (67.1%) SD 14.7%; 2) left gray matter: 12.5 SI units (79.1%) SD 11.7%; 3) white matter: 7.4 SI units (11.2%) SD 2.9%; and 4) sagittal sinus: 282 SI units (1380%) SD 991%. Inclusion of cortical veins within the ROI of cortical gray matter spuriously increased measured enhancement. ROIs that were not purely white or gray matter also altered the measurement. Partial-volume effects at gray-white interfaces decreased measured first-pass enhancement of gray matter and increased measured white matter enhancement.

The times from baseline to peak enhancement were symmetrical for gray matter from side-to-side in each patient. First-order slopes (rise time) of cortical gray matter from baseline to peak were calculated and were symmetrical between hemispheres: 1) right cortical gray matter, 1.35 SI units/sec; 2) left cortical gray matter, 1.34 SI units/sec; 3) white matter, 0.95 SI units/sec. There was a high variance of first-order slope values particularly with white matter since identification of baseline and peak points were difficult.

The ratio of mean signal intensity-time curve of gray matter divided by mean white matter signal intensity-time curve was 1.9. This ratio should reflect the ratio of blood volume in gray matter compared to white matter. This compares well to relative cerebral blood volume ratios of gray matter compared to white matter measured by alternative methods (20).

Gray and white matter %CBVs may be calculated (Table 2). The hemodilution factor of 8 mL of contrast material was considered to be negligible:

Right cortical gray matter = 4.9%, SD = 1.2%
Left cortical gray matter = 4.8%, SD = 1.4%
White matter = 2.6%, SD = 1.1%

These values compare favorably with blood volumes measured by alternative methods (20). There were known sources of error for measurement of cortical gray matter. Partial-volume effects of adjacent cortical veins within ROIs of gray matter elevate calculated %CBV. Likewise, partial-volume effects of the sagittal sinus with adjacent brain tissue lowers measured sagittal sinus enhancement and increases calculated %CBV. Volume averaging of cortical veins was felt to be the most significant source of error during the study. Calculated %CBV of white matter was also adversely affected by volume-average errors of the sagittal sinus.

Subtraction images were obtained of postcontrast scans by subtracting a precontrast baseline scan yielding a first-pass "blood pool" image. The signal intensities of the image approach linearity at concentrations below 1 mmol/L and are closely related to rCBV (Fig. 5). The relative rCBVs are displayed of cortical gray matter and white matter. There is also high signal noted within the lateral ventricles depicting the subependymal and ventricular veins and choroidal blood volumes. Peak enhancement of blood was noted at a gadolinium concentration of 1.8 mmol/L (Fig. 6) for our sequence. The peak enhancement concentration is sequence related. Different degrees of T1 and T2 weighting will cause minor shifts in the

TABLE 1: Absolute and percentile enhancement

Patient No.	Sex	Age	Peak Change SI (%)				
			R Gray Matter	L Gray Matter	White Matter	Dural Sinus	Background
1 EC	M	61	16.3[a] 77.0[b]	17.8[a] 92.2[b]	10.9[a] 15.0[b]	448[a] 881[b]	4.8[c]
2 EW	M	56	10.2 72.0	9.8 80.9	9.2 13.4	273 429	5.1
3 ME	F	39	17.9 80.3	15.6 71.6	7.1 9.7	322 909	4.8
4 MJ	F	53	10.9 61.0	11.4 70.9	5.9 8.2	347 9139	5.0
5 BD	M	28	15.6 74.1	15.1 75.6	9.0 12.7	196 555	4.9
6 CY	F	49	12.6 56.6	15.4 72.4	6.7 9.9	362 1038	5.0
7 SJ	M	48	8.6 43.8	10.3 59.0	5.4 9.1	156 281	5.1
8 DJ	M	52	6.8 47.3	7.1 56.5	8.4 11.3	229 3485	4.8
9 MD	M	34	11.0 58.9	10.6 75.1	6.7 12.3	267 1922	4.8
10 TN	F	54	11.3 72.3	9.6 79.1	6.4 10.1	154 795	4.9
11 BA	F	62	10.6 51.1	12.9 66.8	6.4 11.3	268 2216	5.2
12 SW	M	66	12.2 92.6	12.2 79.4	7.3 11.0	322 1947	5.5
13 LL	M	62	11.1 60.6	12.9 67.4	7.6 11.5	271 492	4.9
14 CW	M	48	12.0 48.5	11.0 47.1	5.6 7.5	328 506	5.2
15 HB	M	58	9.2 54.5	8.7 50.6	7.1 12.0	225 648	4.7
16 FF	F	68	16.9 77.5	16.9 80.7	8.1 10.8	254 698	4.8
17 MJ	M	43	17.1 96.9	16.2 84.3	11.5 18.0	374 3150	4.9
18 DB	F	64	14.8 73.4	13.6 68.0	5.8 9.9	301 1148	5.3
19 MT	F	68	10.0 76.7	10.6 88.2	5.5 9.1	264 1975	4.9
Mean		55	12.4 67.1	12.5 79.1	7.4 11.2	282 1380	5.0
			3.1 14.7	2.9 11.8	1.7 2.9	72.5 991	.2

Note.—R, right; L, left.
[a] Absolute enhancement.
[b] Percent enhancement.
[c] Background signal.

TABLE 2: Percent blood volumes

Patient	R Gray Matter	L Gray Matter	White Matter
1 EC	3.6	3.8	1.6
2 EW	5.0	4.1	2.2
3 ME	5.6	4.5	1.8
4 MJ	6.3	6.2	3.3
5 BD	4.2	4.8	4.4
6 CY	3.5	4.6	1.7
7 SJ	4.5	5.3	2.2
8 DJ	3.3	3.5	4.6
9 MD	6.5	5.4	4.0
10 TN	6.1	5.5	2.1
11 BA	5.8	8.5	4.4
12 SW	5.9	6.1	2.3
13 LL	3.8	4.4	1.8
14 CW	3.9	3.4	1.6
15 HB	5.0	2.7	4.2
16 FF	7.1	5.4	2.5
17 MJ	3.5	2.5	1.6
18 DB	6.2	5.6	1.6
19 MT	3.3	5.8	2.1
Mean	4.9	4.8	2.6
	1.2	1.4	1.1

Note:—R, right; L, left.

peak enhancement versus concentration curve (21).

Discussion

Our results indicate that dynamic MR images obtained by new ultra-fast imaging techniques (Turbo-FLASH, Siemens, Iselin, NJ), in conjunction with a bolus of intravenous gadolinium, allows an assessment of the first-pass brain "blood pool." The regional distribution of the immediate, first-pass enhancement correlates with the regional blood pool or volume. Additionally, an evaluation of vascular hemodynamics may be made. In contrast to echo-planar techniques, Turbo-FLASH requires no "hardware" modification and is available on "general production" scanners.

A heavily T1-weighted image is utilized to maximize relaxivity effects of contrast material. This is obtained by a preparatory nonselective 180° inversion pulse. To achieve maximum contrast enhancement, selection of scan parameters center the central phase encodes in the region of the null point of the targeted tissue. The central phase encoding steps are predominantly respon-

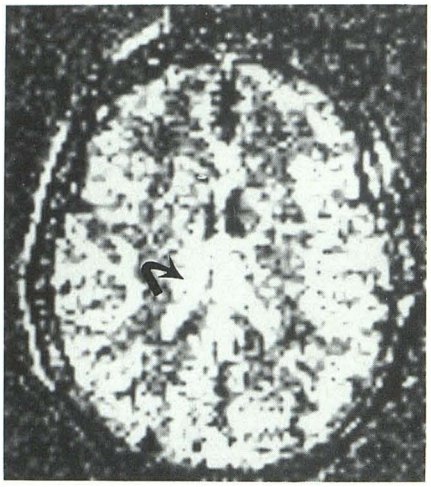

Fig. 5. First-pass blood pool subtraction image depicting the normal pattern of enhancement. There is high signal within the ventricles reflecting the blood volume of the subependymal and ventricular veins and choroid plexus (*arrow*).

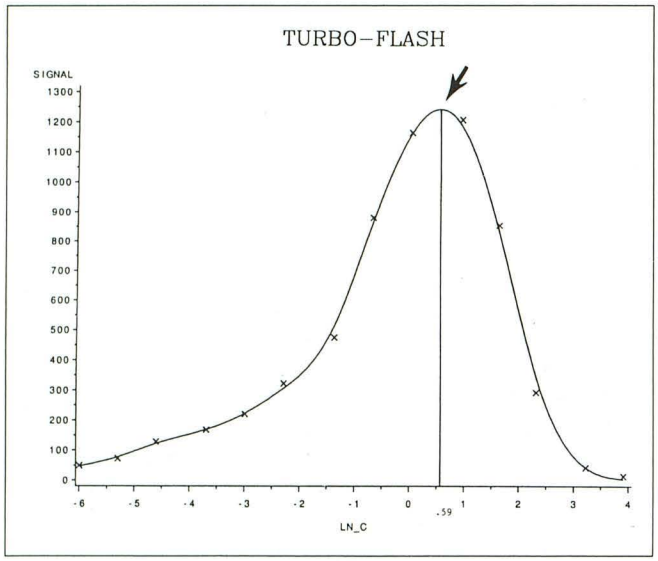

Fig. 6. Graph of MR signal intensity as a function of ln concentration of Gd-DTPA. The peak signal intensity occurs at ln concentration of 0.59 which is 1.8 mmol/L of Gd-DTPA (*arrow*).

sible for image contrast by this method. A partially T2-weighted sequence will diminish the peak enhancement and shift the concentration point where maximum enhancement is realized (21). Percent enhancement and the associated standard deviation are relative values and are quite dependent on the baseline measurement of the signal intensity of the targeted tissue. The absolute change in signal intensity is a more representative figure of enhancement.

The calculated value of percent enhancement is surprisingly dependent on the $SI_{(baseline)}$ in the denominator of equation A. As this value approaches the background signal measurement, very high calculated percent enhancements may be derived. This is somewhat misleading since the change in signal intensity (SI) ($SI_{peak\ enhancement} - SI_{baseline}$) may be minimal. This is equivalent to measuring the tissue signal intensities near the null point of the targeted tissue.

The significant data are actually represented by the magnitude of change of signal of the various tissues relative to each other, rather than percent enhancement which can be altered by changing the pulse sequence to place the signal intensity of the targeted tissue near the null point of the inversion recovery sequence. Baseline values of signal intensity for the SSS are, at times, close to the measured background signal. Low baseline signal intensities or baseline values close to the background signal cause large changes in the calculated percent enhancement and the standard deviations, with small fluctuations of the measured baseline signal intensity. This mathematical manipulation is exemplified by the SSS data in Table 1 (Change SI = 282 ± 72.5 versus %enhancement = 1380% ± 991%). Percent enhancement is directly calculated from the change in SI, yet there are large differences in the magnitude of percent enhancement and, particularly, the relative standard deviations. This is caused by the low baseline signal intensity that, at times, only slightly exceeds the background signal. Hence, the denominator in equation C approaches zero, and the calculated value increases dramatically. This is also germane for calculation of the percent enhancement for gray matter, but is less of a factor for our MR scan sequence.

Hence, relying on percent enhancement only may be misleading. Comparing ΔSIs for gray matter, white matter, and SSS is a more accurate assessment of the regional concentrations of gadolinium contrast agents and rCBV. We have attempted to emphasize ΔSIs in this manuscript rather than percent enhancement, since percent enhancement may be misleading.

Enhancement with paramagnetic materials (ie, transitional and lanthanide metal ions) exert their effects predominantly by dipole-dipole interactions (22). They are nondiffuseable indicators that are normally confined to the intravascular space in the brain. These factors indicate that enhancement is confined to the intravascular space in the brain with little or no enhancement of interstitial or intracellular tissues. The observed enhancement within brain tissue is dependent on contrast material residing within capillaries, venules, and

veins. This volume comprises only approximately 2%–5% of the volume of brain tissue. This method measures both the microcirculation (capillaries and small venules) and macrocirculation (predominantly veins and, to a lesser degree, arteries), and the results should be compared to data obtained by similar methods of measurement.

The change in T1 relaxation time and SI as a function of concentration of the paramagnetic agent are considered to be linear in the peripheral circulation (23). The blood-brain barrier does not modify this relationship. We, similarly, obtained nearly linear responses of T1 relaxation time and signal intensity versus concentration of contrast material in the brain up to a concentration of 1 mmol/L (Fig. 7). Thus, absolute calculations are not possible unless the first-pass bolus concentration of gadolinium in blood is below this level. Standard solutions of gadolinium may be placed within the subject field of view for calibration of SSS concentrations. While there are changes in T1 and T2 relaxivity and magnetic susceptibility with contrast materials, their dipole-dipole interactions or T1 relaxivity effects are accentuated at these concentration levels, and with this heavily T1-weighted sequence.

With new contrast agents there is the potential to use higher doses of paramagnetic agents when they become available for use. Faster rates of injection of contrast material by more centrally placed catheters followed by a saline bolus should provide a more compact bolus; however, large boluses appear to be self-defeating for the T1-weighted method. Higher concentrations of contrast (ie, greater than 1.8 mmol/L) may actually cause a decline in signal intensity by the first-pass method (Fig. 6). These concentration levels are quickly reached even with small amounts of gadolinium agents by central lines or by a compact bolus. A compact bolus gives a better signal intensity versus time profile or compact curve, but smaller quantities of gadolinium agents must be used in order that the 1–2 mmol/L concentration limit is not exceeded. A signal intensity curve generated by a compact bolus of gadolinium by a minimally invasive technique would be preferred as a screening technique in a busy MR imaging center. Thus, the magnitude of enhancement with T1-weighted sequences will also be limited by T2 effects at high concentrations (Fig. 6).

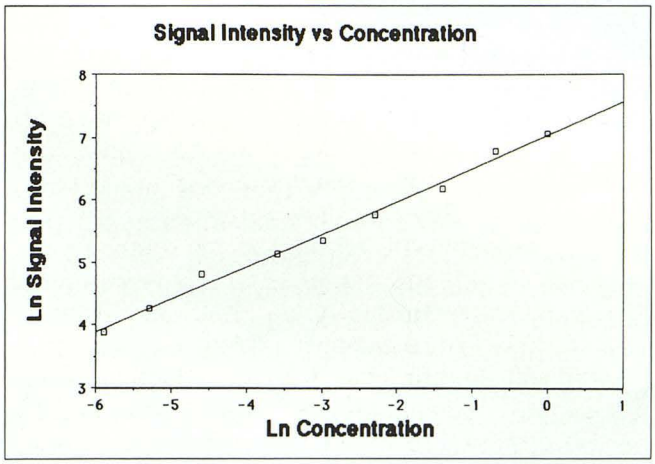

Fig. 7. Graph of ln signal intensity versus ln concentration of Gd-DTPA. There is a nearly linear relationship of concentration versus signal intensity, up to 1 mmol/L. The relationship is no longer linear after 1 mmol/L.

Approximations of CBF which have been described for CT can also be applied to bolus dynamic MR scans (2, 3). These methods are derived from the central volume principle (24) that is derived for nondiffusible indicators such as iodinated contrast and gadolinium contrast agents.

$$CBF = \frac{CBV}{MTT} \qquad (D)$$

This equation assumes a constant volume of cerebral blood. The MTT describes the mean transit time of the indicator through the capillary bed. Reasonable approximations of CBV are derived by measuring tissue signal intensity versus time curves that are equivalent to concentration-time curves at concentrations below 1 mmol/L. Also, absolute values for concentrations of gadolinium in the SSS may be calculated by comparing measured signal intensities with known standards that can be placed within the field of view, and adjusting for signal change related to flow (see equation B). This equation is valid for concentrations less than 1 mmol/L. At the level of the atria and lateral ventricles, the SSS is not truly perpendicular to the axial scanning plane. It is approximately 10° to 15° from perpendicular. The true perpendicular flow vector is, thus, slightly less than the absolute velocity of the SSS. However, this does not appear to be significant, since the range of physiologic velocities are on the plateau of the curve (Fig. 4), and results in no greater change in the signal related to flow effects except at extremely slow velocities. Measurements of SSS flow velocities in normal patients by MR methods yield flow rates of 20–40 cm/sec (Mattle H, abstract SMRM, 1989, 1024).

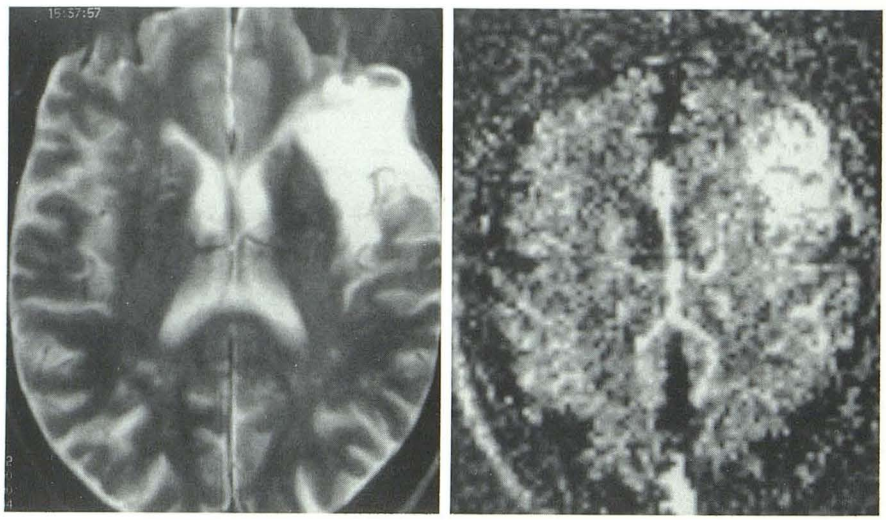

Fig. 8. 10-day-old left frontal lobe infarct with luxury perfusion.

A, T2-weighted image 2500/90/1 demonstrating infarct.

B, Subtraction image depicting increased CBV associated with luxury perfusion.

This method of calculation of CBF (using CBV and MTT) is an estimation and suitable for semiquantitative measurements; however, if imaging times can be further decreased and a compact contrast bolus can be delivered, more accurate measurements would be possible. Scans with imaging times of 1–2 seconds are not suitable for accurate assessment of the transit time or flow. This decrease in imaging time will allow more points on the curve and better estimates of MTT (25). By automating the data analysis and calculating on a per pixel basis, estimated regional CBF images may be possible. Alternatively, this may require a diffusable agent for MR similar to xenon for CT. This would allow a longer data collection interval.

Parallel methods of dynamic enhancement with MR use magnetic susceptibility effects with T2* shortening with delayed echoes on gradient echo images (26, 27). There is greater magnitude of signal alteration with T2* effects, but signal intensity is logarithmically related to the concentration of contrast agent in contrast to the T1-weighted method. By relying on T2* shortening effects there is a loss of signal intensity, with transit of the bolus of contrast material. Various contrast materials have been used, with the best results achieved with contrast agents with high magnetic moments. Signal intensity changes are proportional to the square of the magnetic moment of the contrast material for T2* effects. Higher doses of contrast with new contrast materials should be beneficial with T2*-weighted studies.

While improvements in imaging times are needed to obtain estimates of CBF the first-pass blood pool images may be used to evaluate regional blood pool changes associated with ischemia, trauma, and brain tumors. The evaluation of brain-death may be feasible. Blood pool changes caused by vasodilation and vasoreactivity may be noted in response to ischemia, compressive effects caused by a mass, or trauma. However, these images are most closely related to CBV and not CBF or tissue perfusion.

The presence of luxury perfusion following infarction is readily demonstrated. Luxury perfusion is associated with a decreased MTT and an increased CBV (Fig. 8). Both factors increase the CBF (see equation D). Paradoxically, with the increase in CBF there is an actual decrease in tissue perfusion (1) due to shunting. This high regional CBF associated with luxury perfusion is misleading and the true metabolic and "nutritional" state of the infarct is more accurately evaluated by xenon techniques and PET that more accurately evaluate tissue perfusion and metabolism rather than simply CBF. Also, changes of vasoregulation as depicted by first-pass blood pool subtraction images, frequently, are much more extensive than the infarct demonstrated on the conventional MR images (Fig. 9). Additionally, evaluation of vasoreactive changes in the brain following trauma may be beneficial (Fig. 10).

In summary, significant and measurable first-pass enhancement of both gray and white matter is readily demonstrated with dynamic T1-weighted Turbo-FLASH imaging following a bolus of contrast material. Subtraction images may be obtained to highlight the regional first-pass blood pool. Calculations of %CBV of gray and white matter are possible (cortical gray matter: right

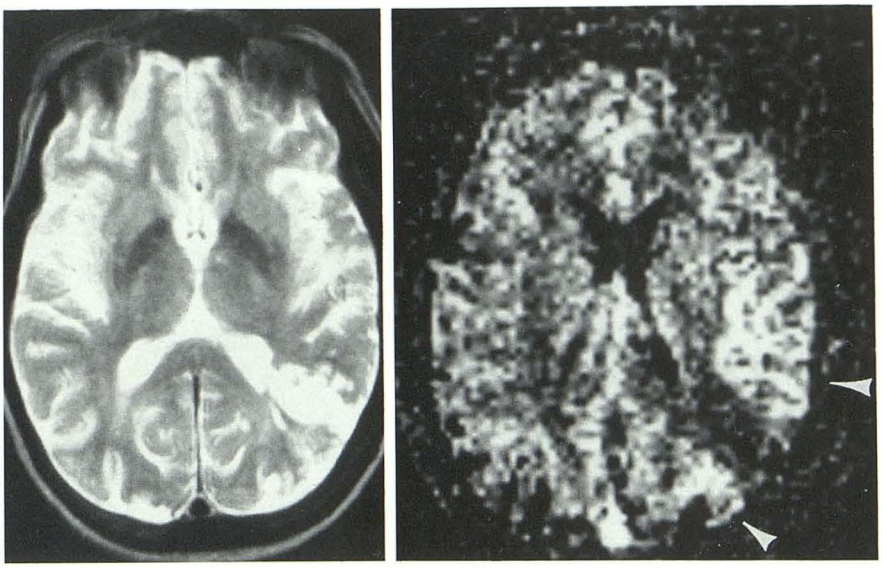

Fig. 9. Small infarct with extensive alteration of vasoregulation.

A, T2-weighted image 2500/90/1. Small left boundary zone infarct.

B, Small hypovolemic area congruous with the infarct noted on T2-weighted sequence. Extensive area of increase in blood-pool (CBV) in the brain surrounding the infarct imaged on the T2-weighted sequence (*arrows*).

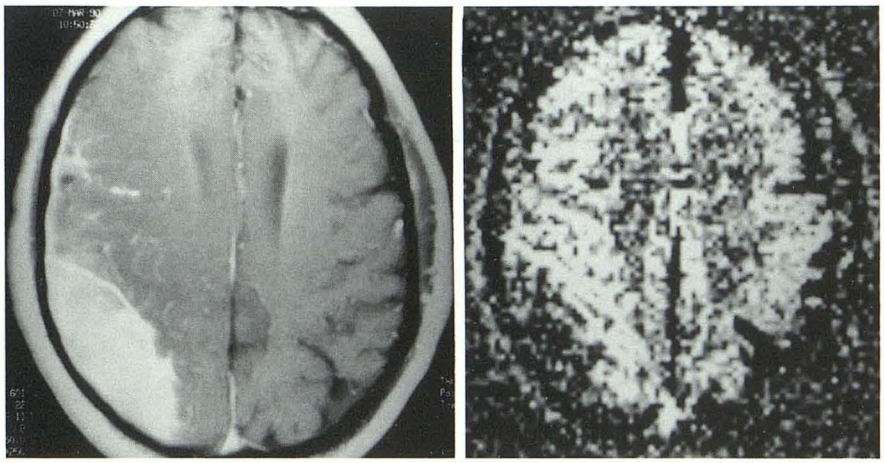

Fig. 10. Response of cerebral blood pool to compression from a subdural hematoma.

A, Subacute subdural with high signal on the T1-weighted image 500/15/2.

B, Subtraction image depicting increased blood pool underlying the subdural hematoma.

4.9%, left 4.8%; white matter: 2.6%) and compare favorably with other methods (20, 28–30). Absolute calculations of CBF by this method may require a more invasive method of contrast injection (arterial injections or central venous injections) and more rapid imaging times. Thus, absolute values for CBF are doubtful by this method for practical use. Reasonable estimates and semiquantitative regional CBF images may be possible, if significant reductions of image acquisition times can be achieved. Initial clinical evaluations of patients with altered intracranial hemodynamics by subtraction blood pool images appear beneficial.

References

1. Drayer BP. Functional applications of CT of the central nervous system. *AJNR* 1981;2:495–510
2. Drayer BP, Heinz ER, Dujovny M, Wolfson SK, Gur D. Patterns of brain perfusion: dynamic computed tomography using intravenous contrast enhancement. *J Comput Assist Tomogr* 1979;3:633–640
3. Norman D, Axel L, Berninger W, et al. Dynamic computed tomography of the brain: techniques, data analysis, and applications. *AJNR* 1981;2:1–12
4. Davis SM, Tress BM, Hopper JL, Kaye AH, Rossiter SC. Dynamic CT brain scanning in the hemodynamic evaluation of cerebral arterial occlusive disease. *Neuroradiology* 1987;29:259–265
5. Heinz ER, Dubois P, Osborne D, Drayer BP, Barret W. Dynamic computed tomography study of the brain. *J Comput Assist Tomogr* 1979;3:641–649
6. Axel L. Cerebral blood flow determination by rapid-sequence computed tomography. *Neuroradiology* 1980;137:679–686
7. Traupe H, Heiss WD, Hoeffken H, Zulch KJ. Hyperperfusion and enhancement in dynamic computed tomography of ischemic stroke patients. *J Comput Assist Tomogr* 1979;3:627–632
8. Drayer BP, Gur D, Wolfson SK, Cook EE. Experimental xenon enhancement with CT imaging: cerebral applications. *AJNR* 1980;134:39–44

9. Touho H, Karasawa K, Nakagawara J, et al. Mapping of cerebral blood flow with stable xenon-enhanced CT and the curve-fitting method of analysis. *Radiology* 1988;168:207–212
10. Hellman RS, Collier BD, Tikofsky RS, et al. Comparison of single-proton emission tomography with [^{123}I]Iodoamphetamine and xenon-enhanced computed tomography for assessing regional cerebral blood flow. *J Cereb Blood Flow Metab* 1986;6:747–755
11. Lassen NA. Measurement of cerebral blood flow and metabolism in man. *Clin Sci* 1982;62:567–572
12. Seeger JF, Carmody RF, Smith JR, Ovitt TW, McNeill K. Evaluation of cerebral hemispheric contrast transit with intravenous digital angiography. *AJNR* 1983;4:333–337
13. Kwan ES, Hall A, Enzmann DR. Quantitative analysis of intracranial circulation using rapid sequence DSA. *AJNR* 1985;7:295–301
14. Hesselink JR, Chang KH, Chung KJ, Abbate L. Flow analysis with digital subtraction angiography: I. Description of a simplified flow model. *AJNR* 1986;7:423–426
15. Hesselink JR, Chang KH, Chung KJ, Abbate L. Flow analysis with digital subtraction angiography: II. Acquisition and accuracy of transit flow measurements. *AJNR* 1986;7:427–431
16. Heiss WD, Herholz K, Bocher-Schwarz HG, et al. PET, CT, and MR imaging in cerebral vascular disease. *J Comput Assist Tomogr* 1986;10:903–911
17. Chugani HT, Phelps ME, Mazziotta JC. Positron emission tomography study of human brain functional development. *Ann Neurol* 1987;22:487–497
18. Knapp WH, Kummer R, Kubler W. Imaging of cerebral blood flow-to-volume distribution using SPECT. *J Nucl Med* 1986;27:465–470
19. Neirinckx R, Canning LR, Piper IM, et al. Technetium-99m d,1-HM-PAO: a new radiopharmaceutical for SPECT imaging of regional cerebral blood perfusion. *J Nucl Med* 1987;28:191–202
20. Greenberg JH, Alavi A, Reivich M, Kuhl D, Uzzell B. Local cerebral blood volume response to carbon dioxide in man. *Circ Res* 1978;43:324–331
21. Davis PL, Parker DL, Nelson JA, Gillen JS, Runge VM. Interactions of paramagnetic contrast agents and the spin echo pulse sequence. *Invest Radiol* 1988;23:381–388
22. Lauffer RB. Paramagnetic metal complexes as water proton relaxation agents for NMR imaging: theory and design. *Chem Rev* 1987;87: 901–927
23. Strich G, Hagan PL, Gerber KH, Slutsky RA. Tissue distribution and magnetic resonance spin lattice relaxation effects of Gd-DTPA. *Radiology* 1985;154:723–6
24. Zierler K. Theoretical basis of indicator-dilution methods for measuring flow and volume. *Circ Res* 1962;10:393–407
25. Axel A. Tissue mean transit time from dynamic computed tomography by a simple deconvolution technique. *Invest Radiol* 1983;18: 94–99
26. Villringer A, Rosen B, Belliveau J, et al. Dynamic imaging with lanthanide chelates in normal brain: contrast due to magnetic susceptibility effects. *Magn Reson Med* 1988;6:164–174
27. Majumdar S, Zoghbi SS, Gore JC. Regional differences in rat brain displayed by fast MRI with superparamagnetic contrast agents. *Magn Reson Imaging* 1988;6:611–615
28. Penn RD, Walser R, Ackerman L. Cerebral blood volume in man: computer analysis of a computerized brain scan. *JAMA* 1975;234:1154–1155
29. Kuhl DE, Reivich M, Alavi A, Nyary I, Staum M. Local cerebral blood volume determined by three dimensional reconstruction of radionuclide scan data. *Circ Res* 1975;36:610–619
30. Grubb RL Jr, Raichle ME, Higgins CS, Eichling JO. Measurement of regional cerebral blood volume by emission tomography. *Ann Neurol* 1978;4:322–328